Monitoring and analysis of snow cover change in an alpine mountainous area in the Tianshan Mountains, China

ZHANG Yin[1,2,3], GULIMIRE Hanati[4], SULITAN Danierhan[1,2*], HU Keke[1,2,3]

[1] State Key Laboratory of Desert and Oasis Ecology, Xinjiang Institute of Ecology and Geography, Chinese Academy of Sciences, Urumqi 830011, China;
[2] Aksu National Station of Observation and Research for Oasis Agro-ecosystem, Aksu 843017, China;
[3] University of Chinese Academy of Sciences, Beijing 100049, China;
[4] Xinjiang Institute of Water Resources and Hydropower Research, Urumqi 830049, China

Abstract: Estimating the snow cover change in alpine mountainous areas (in which meteorological stations are typically lacking) is crucial for managing local water resources and constitutes the first step in evaluating the contribution of snowmelt to runoff and the water cycle. In this paper, taking the Jingou River Basin on the northern slope of the Tianshan Mountains, China as an example, we combined a new moderate-resolution imaging spectroradiometer (MODIS) snow cover extent product over China spanning from 2000 to 2020 with digital elevation model (DEM) data to study the change in snow cover and the hydrological response of runoff to snow cover change in the Jingou River Basin under the background of climate change through trend analysis, sensitivity analysis and other methods. The results indicate that from 2000 to 2020, the annual average temperature and annual precipitation in the study area increased and snow cover fraction (SCF) showed obvious signs of periodicity. Furthermore, there were significant regional differences in the spatial distribution of snow cover days (SCDs), which were numerous in the south of the basin and sparse in the central of the basin. Factors affecting the change in snow cover mainly included temperature, precipitation, elevation, slope and aspect. Compared to precipitation, temperature had a greater impact on SCF. The annual variation in SCF was limited above the elevation of 4200 m, but it fluctuated greatly below the elevation of 4200 m. These results can be used to establish prediction models of snowmelt and runoff for alpine mountainous areas with limited hydrological data, which can provide a scientific basis for the management and protection of water resources in alpine mountainous areas.

Keywords: snow cover fraction; snow cover days; snowmelt runoff; sensitivity analysis; climate change; Jingou River Basin; Tianshan Mountains

Citation: ZHANG Yin, GULIMIRE Hanati, SULITAN Danierhan, HU Keke. 2022. Monitoring and analysis of snow cover change in an alpine mountainous area in the Tianshan Mountains, China. Journal of Arid Land, 14(9): 962–977. https://doi.org/10.1007/s40333-022-0071-3

1 Introduction

As one of the most important natural factors affecting the Earth's surface, snow cover is highly sensitive to climate change and constitutes a vital component of the water cycle (Tan et al., 2019; Kraaijenbrink et al., 2021) with snow cover being the most important freshwater resource in arid

*Corresponding author: SULITAN Danierhan (E-mail: sulitan@ms.xjb.ac.cn)
Received 2022-03-08; revised 2022-06-02; accepted 2022-06-14

areas (Wu et al., 2021). Because of this sensitivity, the spatial and temporal variations of snow cover are closely related to climate change. Indeed, in recent years, precipitation in Xinjiang Uygur Autonomous Region of China has been higher than previously recorded due to global warming. Therefore, because mountainous snowmelt runoff is the main water resource in Xinjiang, it is of great significance to study the change in snow cover under the modern conditions of global warming (Qin et al., 2021).

Previous snow cover research focused mainly on data from ground meteorological stations, whose observations were relatively limited (Yang et al., 2019). However, given the recent development of remote sensing technology, which has become highly effective for snow research, investigations of snow cover have gradually grown from the point scale to the regional and even global scales, with the time series of data having now extended to several decades (Jin et al., 2019; Li et al., 2019; Li et al., 2020; Xiao et al., 2020; Zengir et al., 2020). For instance, Jin et al. (2019) extracted snow cover area (SCA) from a remote sensing dataset as an important input variable for the snowmelt runoff model, thereby compensating for the lack of observation data to a certain extent. Zengir et al. (2020) considered the importance of the role that snowfall plays in supplying water resources, and monitored and analyzed the changes in snow depth (SD) and SCA and their relationships with groundwater in a mountainous area of Iran using remote sensing data; they found that the reduction in the groundwater aquifer is closely related to the decreasing levels of snowfall in the study area. Previous researches have also measured and analyzed remote sensing data to study snow phenology indicators such as SCA, snow cover days (SCDs) and SD in the Tianshan Mountains in Central Asia and in the Northern Hemisphere (Li et al., 2019; Li et al., 2020; Xiao et al., 2020).

As evidenced by the above, the estimation of snowmelt runoff is one of the most important activities of hydrologists (Nagler et al., 2008; Immerzeel et al., 2009; Khadka et al., 2014; Steele et al., 2017). Nagler et al. (2008) developed a data assimilation scheme for predicting short-term runoff. Steele et al. (2017) evaluated the SCA extracted from moderate-resolution imaging spectroradiometer (MODIS) snow cover products, and proposed that all error sources should be fully recognized and understood before using the model to simulate snowmelt runoff to minimize errors. Immerzeel et al. (2009) applied remote sensing technology to analyze the spatial and temporal dynamics of snow cover throughout the river basins of the Himalayas, and used the corrected snowmelt runoff model to analyze the relationships among temperature, precipitation, snow cover and runoff. Khadka et al. (2014) found that approximately 18% of annual runoff in the Tamakoshi Basin could be attributed to the melting of snow and ice during the observation period (2000–2009); they further simulated and predicted the runoff from 2000 to 2059 using the snowmelt runoff model based on a temperature index. The key role that snow plays in the water supply is often quantified using the ratio of snowmelt runoff to the total runoff; for instance, on the basis of a hydrological model simulation and a new snowmelt tracking algorithm, Li et al. (2017) found that 53% of the total runoff in the western United States originates from snowmelt, and in mountainous areas, snowmelt runoff accounts for 70% of the total.

In mountainous areas, seasonal snow stores water in winter and melts in spring and summer to replenish agricultural, industrial and urban water resources downstream. Particularly in arid and semi-arid regions characterized by the limited availability of such water resources, the potential impact of climate change is a major concern for water resource managers. The generation of runoff and the recharge of deep groundwater may be affected by snow loss (Hammond et al., 2019). Tang et al. (2019) implemented a coupled hydroecological simulation system and found that the snowmelt variation caused by climate change can account for more than 60% of the annual runoff change in the Great Basin of North America. Thus, climate change-induced snowfall variations are of considerable significance to managing the annual distributions and availability of water resources in arid and semi-arid regions. In particular, Moursi et al. (2017) proposed that under climate change, the probability of water shortages in semi-arid and snowmelt-dominated river basins is quite high, and corresponding policies need to be implemented.

The Jingou River Basin (JRB) is located on the topographically complex northern slope of the

Tianshan Mountains at a high elevation. Because there are no snow monitoring stations in this basin, remote sensing data are crucial for obtaining the snow parameters for this area. In the application of hydrological models, the spatial information of snow can be used as input variables (Tahir et al., 2011a, 2017; Zhang et al., 2014). In this context, the purpose of this study was to explore the snow cover change in the JRB in recent years using remote sensing data. Snow cover fraction (SCF) data obtained from a new MODIS snow cover extent product for China were obtained to analyze the relationships between SCF and climate factors, determine the correlation between SCF and runoff and quantify the response of runoff to SCF change in the JRB. The influencing factors of snow cover change in the JRB under climate change were also explored. This study can provide a reference for the research of snow cover in alpine mountainous areas and help to compare and evaluate snowmelt model simulations and future snowmelt runoff predictions.

2 Materials and methods

2.1 Study area

The Jingou River (85°03′–85°44′E, 43°30′–44°50′N) is located within the Xinjiang Uygur Autonomous Region of China and its basin is located on the northern slope of the Tianshan Mountains and on the southern edge of the Junggar Basin. The river originates from the glacial area on the north side of the Eren Habirga Mountain, flows from south to north into the alluvial plains and eventually enters the Manas River as its first tributary. The terrain of the JRB is high in the south (with the highest elevation of 5152 m) and low in the north (with the lowest elevation of 1243 m). The annual average temperature is 5.2°C, and the average annual precipitation is 284.5 mm. The Jingou River is a typical glacial melting and snowmelt river. There are 120 glaciers in the JRB and snowmelt accounts for 34% (1.23×10^8 m^3) of the surface runoff in the basin. The total annual runoff within the basin reaches approximately 3.83×10^8 m^3, and the annual variation in runoff is quite pronounced, with the runoff from June to August accounting for 70% of the annual total (Chen et al., 2017). This study takes the upstream of the Bajiahu hydrological station in the JRB as the study area (Fig. 1), covering an area of 1175.67 km^2.

2.2 Digital elevation model (DEM) dataset

The DEM data used in this study were downloaded from the Geospatial Data Cloud (http://www.gscloud.cn/sources/accessdata/305) and extracted from the Shuttle Radar Topography Mission (SRTM) DEM with a spatial resolution of 90 m. We used ArcGIS for mosaic analysis after downloading the data; then, based on the stitched images, we performed a series of operations, such as filling, flow direction analysis and flow accumulation processing, and finally generated the basin boundary.

2.3 Runoff data and meteorological data

Considering the limited availability of data, we used daily runoff data during the period of 2006–2019 from the Bajiahu hydrological stations in the JRB. The meteorological data (1964–2020) were downloaded from the National Meteorological Information Center of the China Meteorological Administration (http://data.cma.cn/data). Temperature and precipitation data were interpolated from three meteorological stations (Paotai, Wulanwusu and Shawan; Fig. 1) at different elevations (337, 468 and 522 m, respectively) within the JRB.

2.4 Snow cover product

In this study, a new daily, cloud-free MODIS snow cover extent product over China during the period of 2000–2020 was used for analyzing snow cover (Hao, 2021), and the dataset was downloaded from the National Tibetan Plateau/Third Pole Environment Data Center (https://data.tpdc.ac.cn/en/). Based on the MOD/MYD09GA MODIS reflectivity product, we prepared the dataset using a high-resolution Landsat TM dataset as the ground true, which

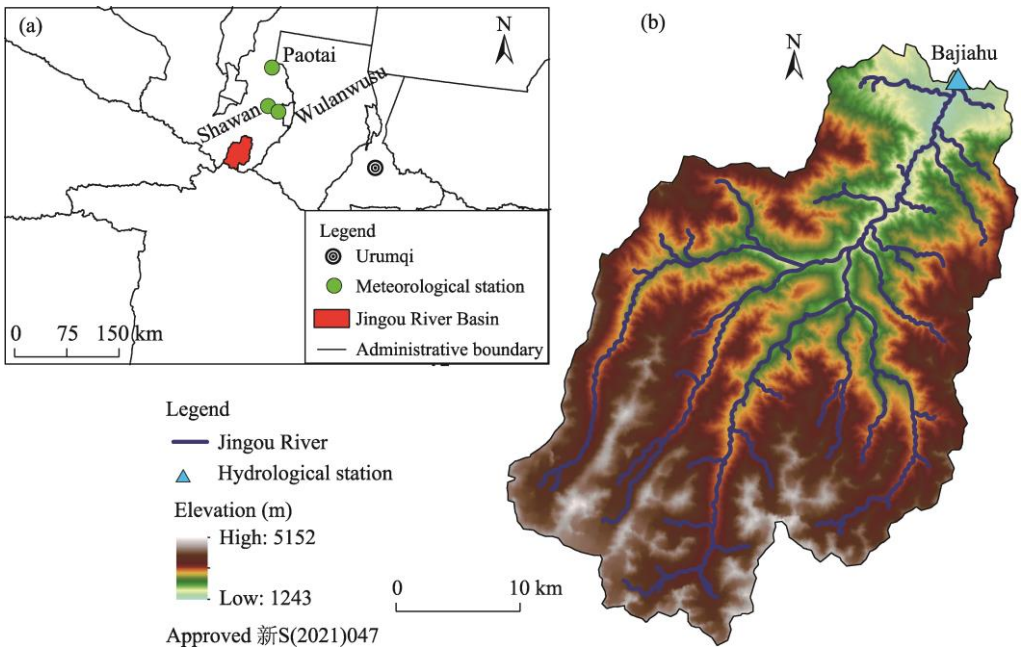

Fig. 1 Location of the Jingou River Basin (JRB) and distribution of the meteorological stations (a), and the overview of the JRB. Note that the figures are based on the standard map (新 S(2021)047) of the Map Service System (https://xinjiang.tianditu.gov.cn/main/bzdt.html) marked by the Xinjiang Uygur Autonomous Region Platform for Common Geospatial Information Services, and the administrative boundaries are not modified.

was combined with a decision tree algorithm for identifying snow on different surface types to obtain the primary product. Through a spatiotemporal interpolation algorithm for the hidden Markov random field model, we filled data gaps, removed clouds and then obtained the daily cloud-free snow product with a spatial resolution of 500 m.

MOD10A2 V06 and MYD10A2 V06 data, which were generated by extracting the 8-d maxima of MOD10A1 and MYD10A1 tiles, were used to obtain SCDs within the JRB with a spatial resolution of 500 m. Compared to MOD10A1 and MYD10A1, MOD10A2 and MYD10A2 can greatly reduce the impact of clouds with an absolute accuracy of approximately 93% (Hall and Riggs, 2010), which have been widely used to calculate SCF in mountainous areas with complex terrain (Tahir et al., 2011b; Zhang et al., 2020).

In this paper, we collected 825 MOD10A2 scenes and 827 MYD10A2 scenes (https://search.earthdata.nasa.gov/search) from 2003 to 2020 (MOD10A2 data missing: 2003353, 2008113 and 2016049; MYD10A2 data missing: 2020233). Using the MODIS Reprojection Tool (MRT) tool and Python programming language, we carried out several operations, including mosaicking, formatting, projection conversion and clipping, among others. The maximum function was used to calculate the image composite (the principle is similar to the synthesis algorithm of MOD10A2 and MYD10A2) as follows:

$$S_{(y,x,t)} = \max\left(S^{T}_{(y,x,t)}, S^{A}_{(y,x,t)}\right), \tag{1}$$

where y and x are the row and column indices, respectively; t is the index for the day of pixel S; and S^T and S^A represent the Terra and Aqua pixels, respectively. Cloud cover can be reduced by merging the two groups of images from the same time (Paudel and Andersen, 2011). When either Terra or Aqua data were not available on a certain day, fusion was not carried out, and MOD10A2 or MYD10A2 data were directly used as the fusion result for the next operation.

2.5 Trend analysis

The Mann-Kendall (M-K) method was used to test for abrupt changes in climate elements (Mann,

1945; Kendall, 1990) and was realized based on MATLAB. The principle is to construct a rank sequence S_k for time series X to reflect the cumulative value of the preceding values when the value of the i^{th} moment is greater than that of the j^{th} moment. During each mutation test, the above process is repeated in the reverse order of the time series. Under the assumption of random time series, statistics of UF_k and UB_k are defined as follows (Yue et al., 2002):

$$UF_k = \frac{[S_k - E(S_k)]}{\sqrt{\mathrm{Var}(S_k)}} (k=1, 2, \ldots, n), \tag{2}$$

$$UB_k = -UF_k (k=n, n-1, \ldots, 1), \tag{3}$$

where UF_k and UB_k are two statistics in M-K test, which are used to determine the upward and downward trends and the location of the abrupt change point, with UF_1=0; and $E(S_k)$ and $\mathrm{Var}(S_k)$ are the mean and variance of S_k, respectively. When the value of UF_k or UB_k is greater than zero, the sequence shows an upward trend; otherwise, the sequence shows a downward trend. At a significance level of 0.05, the critical value is ±1.96; if UF_k or UB_k exceeds this critical threshold (±1.96), there is a significant upward or downward trend. If there is an intersection point between the UF_k and UB_k curves and the intersection point is within the significance interval, the intersection point is a mutation point (or an inflection point). The change trends of the time series before and after such a mutation point are always reversed.

2.6 Sensitivity analysis

Snow cover variations directly impact rivers fed by snow or glacial meltwater in mountainous areas. As temperature rises in spring, snow begins to melt, and runoff increases accordingly. Therefore, a sensitivity model was adopted to quantify the hydrological response of runoff to SCF variations (Kour et al., 2016):

$$\varepsilon\ (S,Q) = \frac{\bar{S}}{\bar{Q}} \frac{\sum (S_i - \bar{S})(Q_i - \bar{Q})}{\sum (S_i - \bar{S})^2}, \tag{4}$$

where ε is the sensitivity coefficient of SCF to monthly runoff; S (%) is the SCF (snow cover fraction); Q (m^3/s) denotes the monthly runoff; S_i (%) is the snow cover fraction of the i^{th} month; Q_i (m^3/s) is the monthly runoff of the i^{th} month; and $\bar{S}$ and $\bar{Q}$ are the monthly mean SCF and monthly runoff from 2006 to 2019, respectively. ε shows that an SCF change of 1% can lead to a ε% change in runoff.

3 Results

3.1 SCF variation characteristics

Figure 2a shows the change in SCF throughout the study area from 2000 to 2020. The periodicity of snow cover in the JRB is obvious. Each year featured a complete snow accumulation period and snow melting period. Snow began to fall at the end of August every year, and snow cover began to increase rapidly beginning in September. From December to the end of February of the following year, snow area reached its maximum, with the peak generally occurring in February, and snow melted beginning in March until the end of August. The maximum SCF was 66.13%, while the minimum SCF was 6.14%. The minimum annual mean SCF was 31.37% in 2020, and the maximum annual mean SCF reached 44.92% in 2010. From 2000 to 2020, SCF in the basin showed a slight downward trend, at the rate of –0.2%/10a (Fig. 2b).

3.2 Spatiotemporal variation in SCDs

According to the spatiotemporal variation in SCDs in the JRB from 2003 to 2020 (Fig. 3), it can be seen that snow cover was widely distributed. However, under the influences of climate, elevation and other factors, there were obvious regional differences in SCDs. The southern part of the basin exhibited a high elevation and low temperature, which are conductive to the continuous development of snow cover. Hence, this area featured relatively stable and high numbers of SCDs

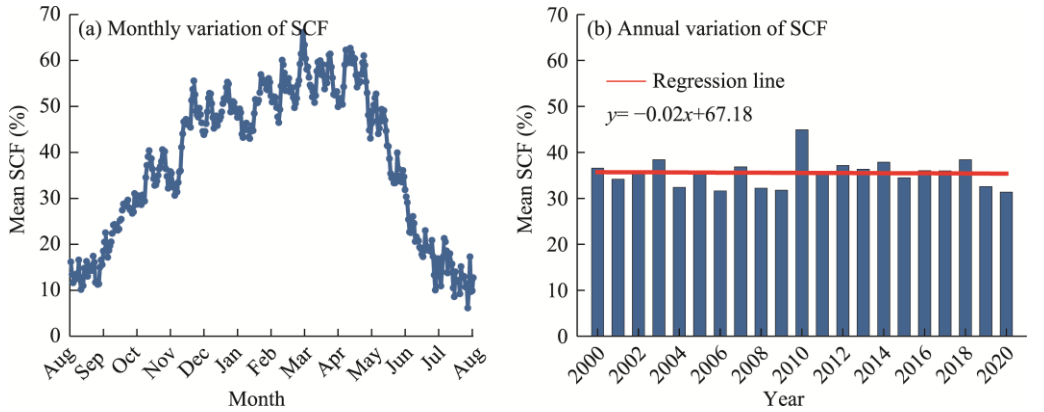

Fig. 2 Monthly variation of SCF (a) and annual variation of SCF (b) from 2000 to 2020 in the JRB. SCF, snow cover fraction.

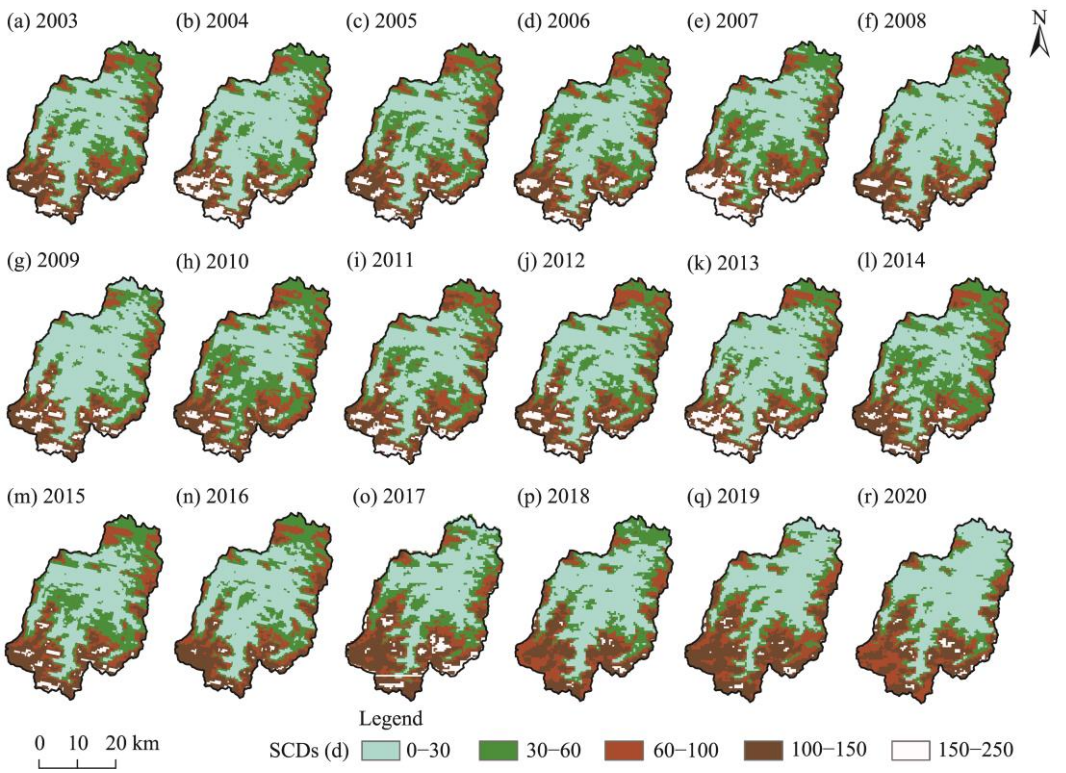

Fig. 3 Spatiotemporal variations of snow cover days (SCDs) from 2003 to 2020 in the JRB

in the basin (a 'stable' SCA refers to an area with continuous snow cover for longer than one month, while an 'unstable' SCA refers to an area with snow cover for less than one month). Except for a few unstable SCAs in the central section of the JRB, the other areas were seasonally and stably covered with snow, and the overall trend changed little during the study period.

To further analyze the spatiotemporal distributions of SCDs in the JRB, we calculated the multiyear mean and standard deviation of SCDs (Fig. 4). At the spatial scale, SCDs increased from the north to the south of the JRB. Under the influence of elevation, SCDs in the basin presented a typical vertical zonal distribution, with the number of SCDs gradually increasing from low to high elevations. High SCD values were concentrated mainly in the southwestern and southern areas at higher elevations, with the values exceeding 150 d. According to Figure 4b, little has changed during the study period, although the standard deviation was quite large in some

high-elevation areas in the south, where the numbers of SCDs have changed considerably. Nevertheless, the standard deviation was small and stable in most other areas.

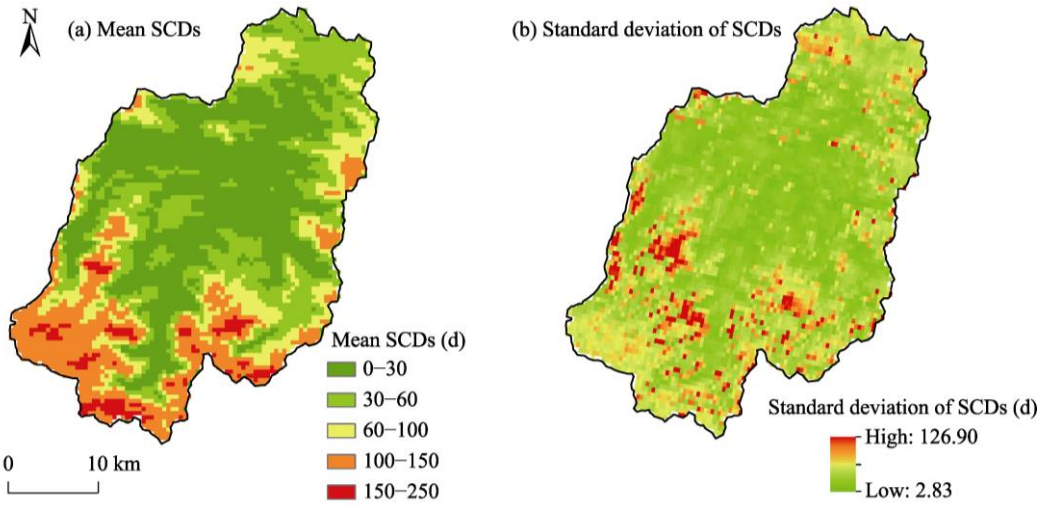

Fig. 4 Spatial distributions of mean SCDs (a) and standard deviation of SCDs (b) from 2003 to 2020 in the JRB

3.3 Factors driving snow cover change in the JRB

3.3.1 Impact of climate change on snow cover change

Changes in the air temperature and precipitation have played a key role in snow cover change in the JRB, as snowfall and low temperature are required for snow accumulation. The variation characteristics of the annual average temperature and annual precipitation in the study area are shown in Figure 5. From 1964 to 2020, the annual average temperature in the JRB was greater than 0.0°C and the annual precipitation was greater than 300.0 mm, with both showing an upward trend.

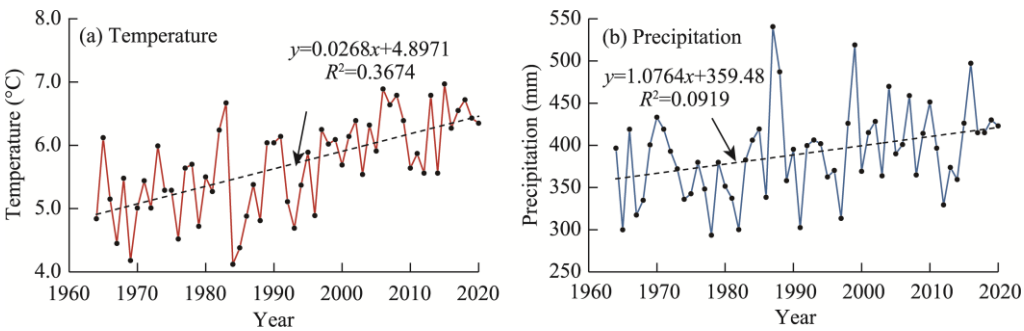

Fig. 5 Variations in the annual average temperature (a) and annual precipitation (b) from 1964 to 2020 in the JRB

Furthermore, the M-K method was used to test for abrupt changes of temperature and precipitation data (Fig. 6). The results show that the annual average temperature in the basin increased obviously during the period of 1964–1966, but the increase was not significant. Specifically, the annual average temperature has continued to increase since 1972. The UF_k value exceed the critical threshold in 2000, when temperature began to increase significantly. We found that the UF_k and UB_k curves intersected within the confidence level interval, and the mutation year was determined to be 1998 according to the location of this intersection point (Fig. 6a). In addition, there was an obvious increase in the annual precipitation during the period of 1968–1977 in the basin, and the annual precipitation continued to increase after 1986, with a significant increasing trend beginning in 2006 (Fig. 6b).

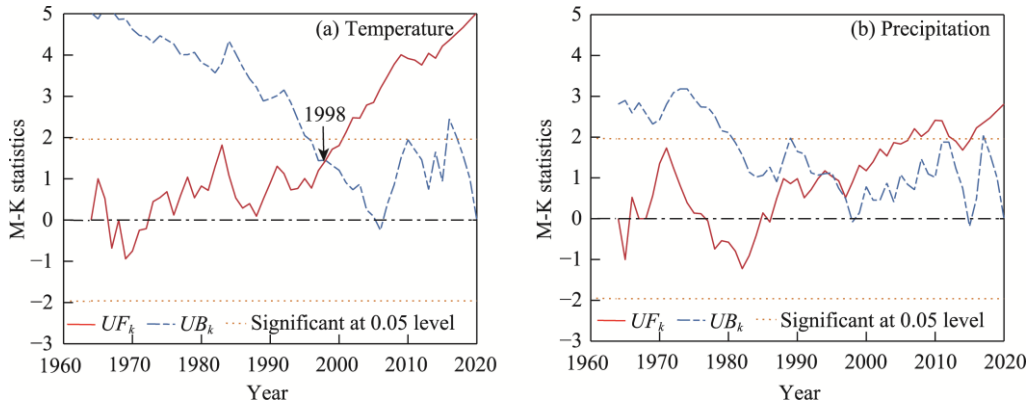

Fig. 6 Mann-Kendall (M-K) tests of the annual average temperature (a) and annual precipitation (b) from 1964 to 2020 in the JRB. UF_k and UB_k are two statistics in M-K test, which are used to determine the upward and downward trends and the location of the abrupt change point.

This study focused mainly on the period after 2003, during which temperature and precipitation increased significantly, especially the former. To study the impact of climate change on snow cover, we selected four factors, namely, monthly mean temperature, monthly total precipitation, previous monthly mean temperature and previous monthly total precipitation, to establish the following multiple linear regression model:

$$\mathrm{SCF} = -0.40T_i + 0.01P_i - 0.77T_{i-1} - 0.01P_{i-1} + 32.39\,, \tag{5}$$

where SCF is the snow cover fraction (%); T and P denote temperature (°C) and precipitation (mm), respectively; i denotes the temperature and precipitation of the current month; and i–1 denotes the temperature and precipitation of the previous month. Equation 5 shows that SCF in the basin was negatively correlated with the monthly mean temperature, the previous monthly mean temperature and the previous monthly total precipitation, with coefficients of –0.40, –0.77 and –0.01, respectively. In contrast, SCF was positively correlated with the monthly total precipitation, with a coefficient of 0.01. Overall, temperature had a greater impact than precipitation on the snow cover extent. Nevertheless, in the JRB, which includes a typical river fed by glacial melting and snowmelt, snow cover change exhibited a fundamental relationship with the temperature and precipitation, and the fitting effect was satisfactory with a coefficient of determination (R^2) of 0.63.

3.3.2 Impact of elevation on snow cover change

Snow cover change in the JRB was closely related to elevation (Wang et al., 2008). In this study, the study area was divided into seven elevation zones at intervals of 500 m (sequentially numbered E1–E7): 1243–1700, 1700–2200, 2200–2700, 2700–3200, 3200–3700, 3700–4200 and 4200–5152 m, respectively. Due to the long time series and large number of maps involved, a snow image of the JRB taken on 18 March 2008, was used as an example (Fig. 7a). After superimposing this snow image onto these DEM classification maps, snow data map for each elevation zone in the basin was obtained (Fig. 7b).

Based on the results, we further derived the snow cover data for each zone to calculate the SCF of each elevation zone from 2000 to 2020, as shown in Figure 8. In terms of the annual SCF change, the change rates of SCF in the five elevation zones (shown in Fig. 8a–e) were similar. The SCF fluctuated greatly in the low-elevation zones and was sensitive to temperature. Moreover, SCF in each of the five elevation zones varied by season. Specifically, SCF was the highest in winter, decreased with the arrival of spring, reached the lowest level after the end of the summer snowmelt period, and then gradually increased in autumn. There was little snow cover in summer. With an increase in elevation, the fluctuation range of SCF decreased, and the snow accumulation period and snowmelt period lengthened. The variation of SCF was the highest in the elevation range of 1243–1700 m.

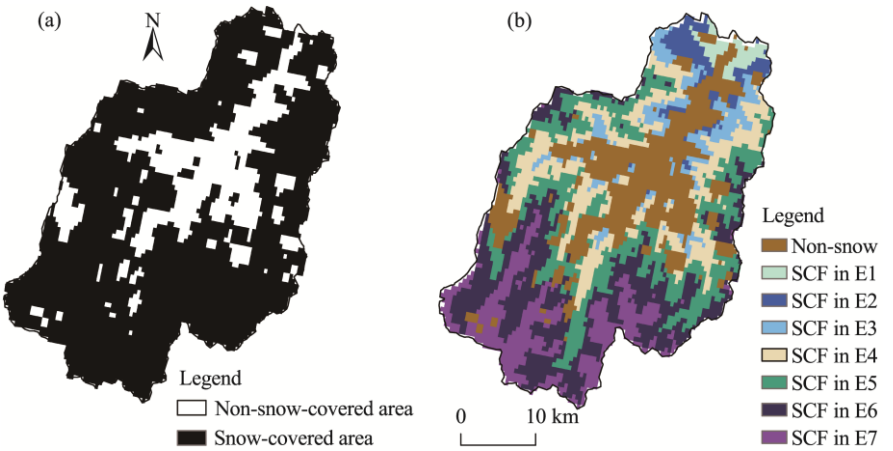

Fig. 7 Distribution of snow cover from an image taken on 18 March 2008 (a) and the composite image of SCF for the seven elevation zones (b) in the JRB. E1–E7 respectively refer to the seven different elevation zones: 1243–1700, 1700–2200, 2200–2700, 2700–3200, 3200–3700, 3700–4200 and 4200–5152 m.

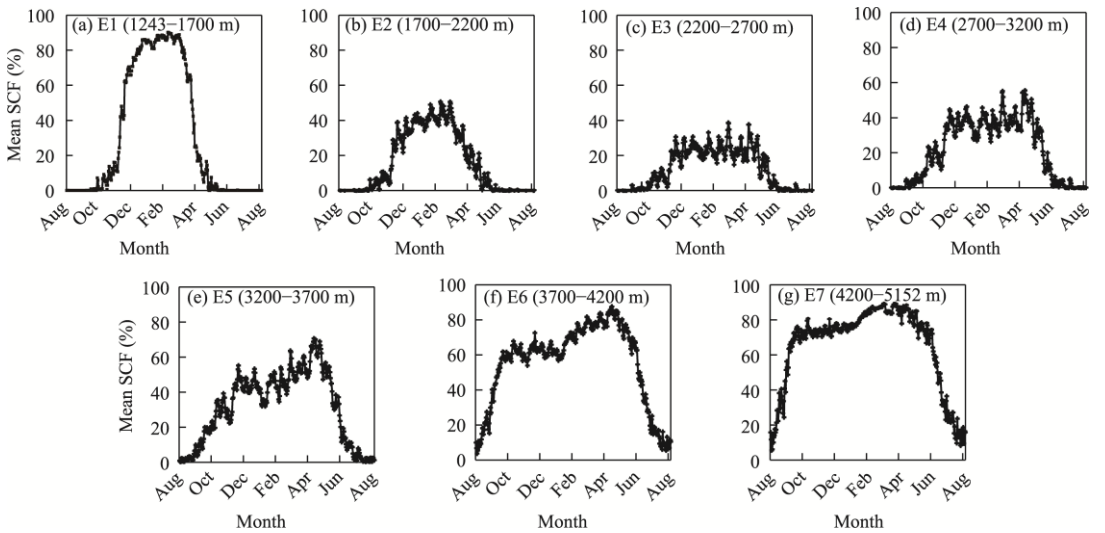

Fig. 8 Variations of monthly mean SCF in the different elevation zones (a–g) from 2000 to 2020 in the JRB

In contrast, above an elevation of 4200 m (Fig. 8g), where the snow cover was stable, the monthly variation of SCF was relatively limited, as SCF was affected by annual snow (glaciers) in the high-elevation zones.

In terms of annual SCF change, SCFs in the E5–E7 elevation zones showed upward trends, while SCFs in the E1–E4 elevation zones exhibited downward trends (Fig. 9), with tends of –0.36%/10a, –0.25%/10a, –0.11%/10a, –0.20%/10a, 2.03%/10a, 3.03%/10a and 5.19%/10a in the E1–E7 elevation zones, respectively. Hence, the change rate of SCF was low in the lower-elevation zones and high in the higher-elevation zones. Among these measures, the rate of increase in the 4200–5152 elevation zone was the highest, at 5.19%/10a. As high-elevation zones are composed of mostly permanent snow (glaciers), these areas are extremely sensitive to climate change and are obviously affected by global warming.

3.3.3 Impacts of slope and aspect on snow cover change

In addition to elevation, due to the windward and leeward effects, slope and aspect can affect the change of SCF by altering the local solar radiation and humidity conditions. To study the impacts of slope and aspect on snow cover change, we superimposed the snow cover, slope and aspect data to obtain snow cover data with different slopes and aspects using the same method described in Section 3.3.2.

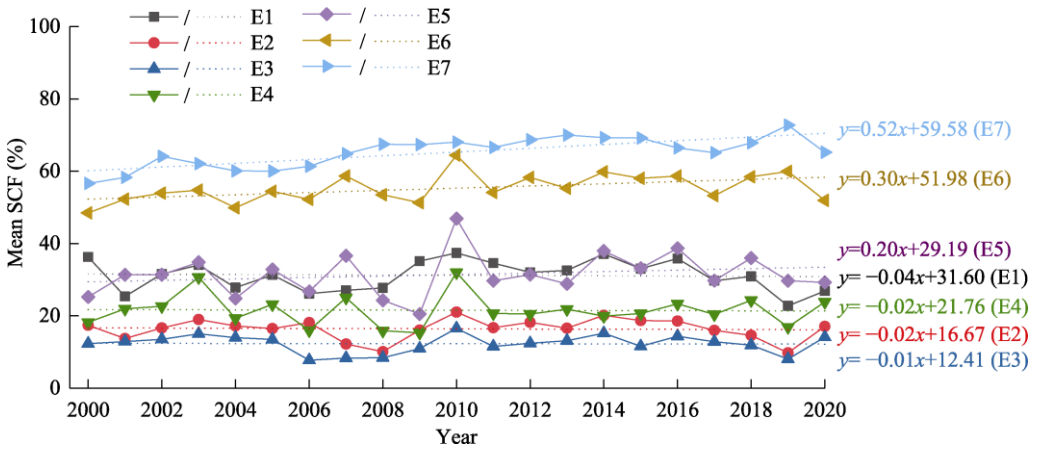

Fig. 9 Variations of annual mean SCF in the different elevation zones (E1–E7) from 2000 to 2020 in the JRB. The dotted lines represent the linear trends.

The impact of slope on snow cover change is illustrated in Figure 10. Slopes of 0°–10° were more conducive to snow accumulation, and SCF maintained a high value and fluctuated considerably by season; the corresponding annual average SCF was 54.20%. Slopes of 30°–40° and 40°–90° were not conducive to snow cover, and SCF followed a similar trend throughout the year, with SCF remaining low and exhibiting gentle seasonal fluctuation. This may be because snow cover was also related to other factors such as aspect. In addition, vegetation type affected the variations of SCF (snow melts faster on bare land and slower in areas covered with vegetation).

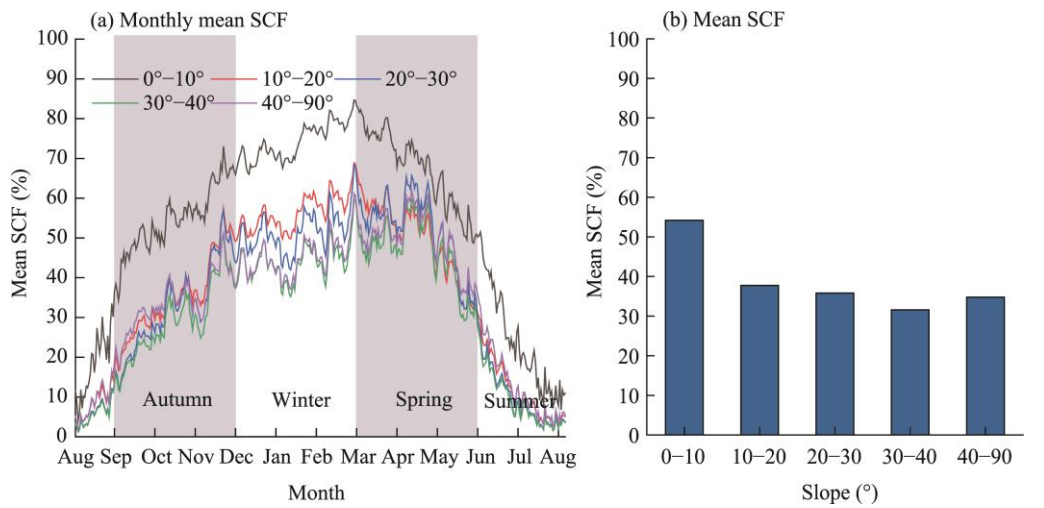

Fig. 10 Variations of monthly mean SCF on the different slopes at the annual scale (a) and mean SCF of different slopes (b) from 2000 to 2020 in the JRB. Spring, March, April and May; Summer, June, July and August; Autumn, September, October and November; Winter, December, January and February.

In terms of its interannual variations, SCF in the 0°–10° and 10°–20° slopes showed upward trends, whereas SCF in the other slopes showed downward trends (Fig. 11), with increasing tends of 2.56%/10a, 0.56%/10a, –0.24%/10a, –0.06%/10a and –0.06%/10a in the slopes of 0°–10°, 10°–20°, 20°–30°, 30°–40° and 40°–90°, respectively. The change rate of SCF was higher on gentler slopes and lower on steeper slopes. Among them, the increasing rate of SCF in the 0°–10° slopes was the highest under climate change and SCF value reached its highest value in 2010.

The impact of aspect on snow cover change is plotted in Figure 12. SCFs on the west- and north-facing aspects (including northwest, north and northeast) were relatively high, with small

fluctuations occurring throughout the year. In contrast, SCFs on the south-facing aspects (including south and southwest) were low and fluctuated greatly within each year. We assumed that the south-facing areas were more vulnerable to higher levels of solar radiation, increasing snowmelt therein and reducing SCF. In addition, the study area is located on the northern slope of the Tianshan Mountains, where most precipitation falls on windward (west and northwest) slopes, which is also conducive to snow accumulation (Li et al., 2020). In winter, SCF differed considerably among the eight aspects (north, northeast, east, southeast, south, southwest, west and northwest); the maximum value was found on a west-facing aspect, while the minimum value was found on a south-facing aspect. In contrast, the difference was small in summer, and the minimum SCF was recorded on a southwest-facing aspect, indicating that snow melted fastest on the southwest-facing aspect in summer.

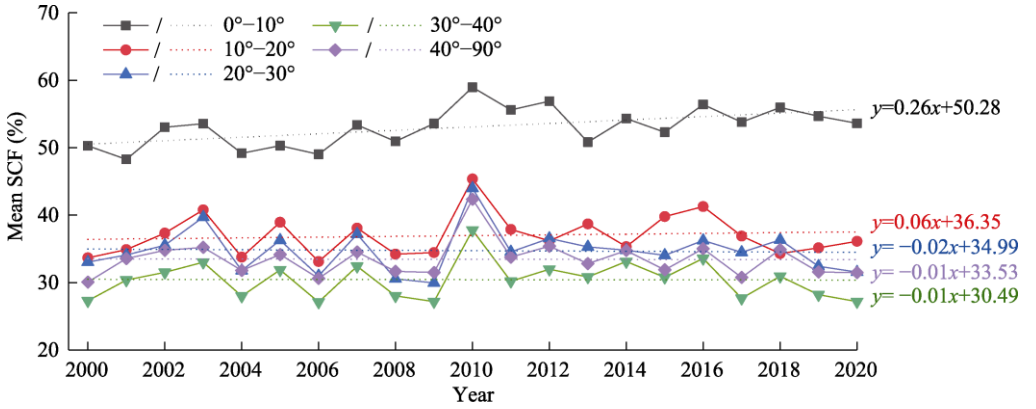

Fig. 11 Variations of annual mean SCF on the different slopes from 2000 to 2020 in the JRB. The dotted lines represent the linear trends.

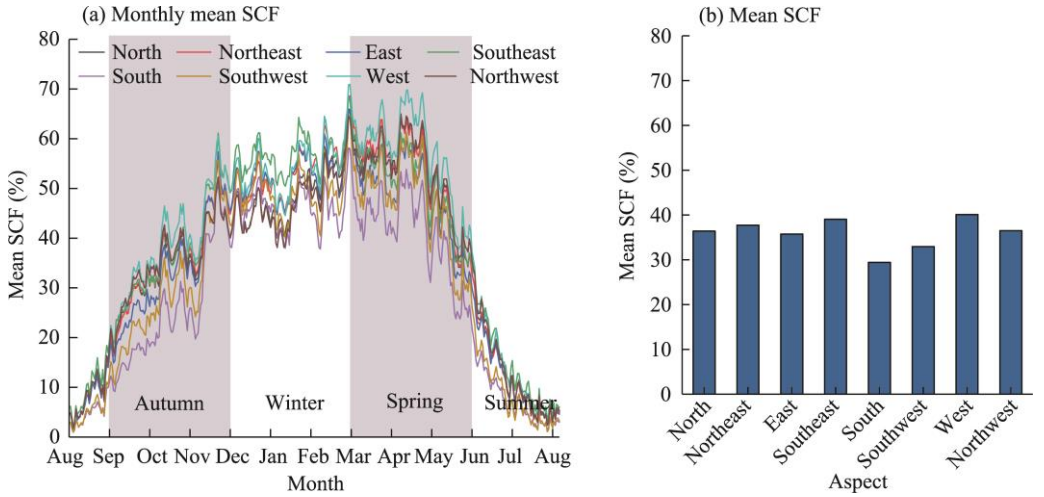

Fig. 12 Variations of monthly mean SCF on the different aspects at the annual scale (a) and mean SCF of different aspects (b) from 2000 to 2020 in the JRB

In terms of interannual change in SCF, the values on the north- and northeast-facing aspects showed upward trends, while those on the other aspects exhibited slight downward trends overall (Fig. 13). The tends of SCF change on the eight aspects (north, northeast, east, southeast, south, southwest, west and northwest) were 1.34%/10a, 1.52%/10a, –0.31%/10a, –0.05%/10a, –0.16%/10a, –0.37%/10a, –0.08%/10a and –0.09%/10a, respectively. The change rate of SCF on the northeast-facing aspect was higher than that on the other aspects; further, the basin was wetter in 2010 than in other years, and SCF value was the highest in this year.

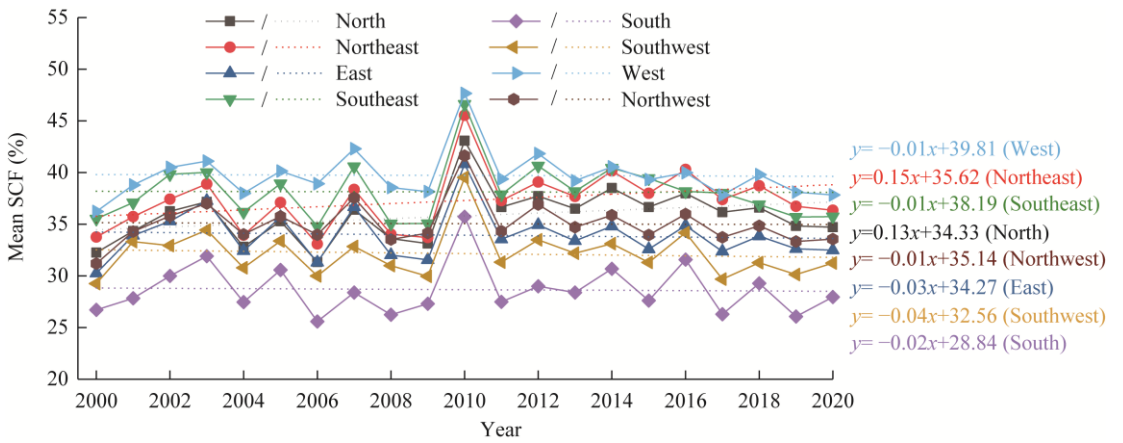

Fig. 13 Variations of annual mean SCF on the different aspects from 2000 to 2020 in the JRB. The dotted lines represent the linear trends.

4 Discussion

4.1 Hydrological response of runoff to snow cover change

In arid and semi-arid areas, water derived from the melting of snow and ice is the main source of riverine recharge (Li et al., 2013; Miller et al., 2021; Saeed et al., 2022). In the context of global warming, snow and glaciers melt rapidly, which increases streamflow, resulting in many snowmelt-based flood events (Liu et al., 2015; Uwamahoro et al., 2021). Therefore, it is necessary to study the hydrological response of runoff to snow cover change.

In this study, we compared the runoff and SCF variations in the JRB from 2006 to 2019. According to observations, the variations in runoff were significantly negatively correlated with the change in snow cover at the 0.01 significance level (Table 1). The appearance of each discharge peak was significantly related to snowmelt, and the maximum discharge peak appeared at the end of August. Parajka et al. (2019) also conducted a detailed study on a large number of runoff events in Europe and found that the occurrence of flood peaks was closely related to the occurrence of snow melting events; they also pointed out that most basins in Europe experienced 3–6 snowmelt-based runoff events every year and the number of occurrences was positively related to the maximum elevation of the basin. Our study also found that the peak runoff has decreased and the timing of the peak has advanced in recent years (Fig. 14). With increasing summertime air temperature, snow has melted with increasing intensity, and the surface and underground runoff has converged into the mountain passes, increasing runoff therein. Thus, fluctuations in SCF had a significant effect on the runoff response within the basin.

Table 1 Correlation between snow cover fraction (SCF) and runoff from 2006 to 2019 in the Jingou River Basin (JRB)

Year	*r*	Year	*r*
2006	–0.64**	2013	–0.59**
2007	–0.74**	2014	–0.69**
2008	–0.60**	2015	–0.70**
2009	–0.58**	2016	–0.73**
2010	–0.77**	2017	–0.65**
2011	–0.68**	2018	–0.77**
2012	–0.74**	2019	–0.74**

Note: *r*, correlation coefficient. ** indicates that the correlation is significant at the 0.01 level.

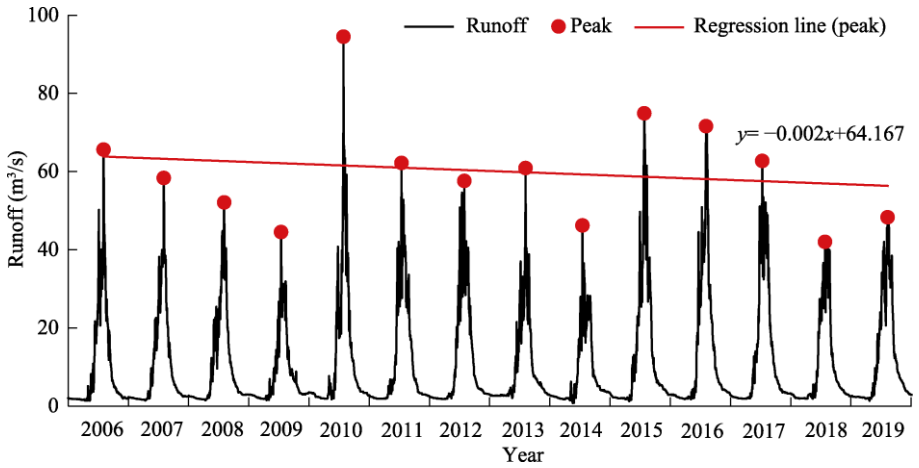

Fig. 14 Daily runoff time series from 2006 to 2019 in the JRB

4.2 Sensitivity analysis

The annual runoff in the JRB is affected mainly by snowmelt, and the JRB includes a typical snowmelt-recharged river. To quantify the impact of SCF on monthly runoff, we calculated the sensitivity coefficient between SCF and runoff (Fig. 15).

Overall, the range of the sensitivity coefficients of SCF to monthly runoff was from –0.64 to 0.07 during the period of 2006–2019, and annual fluctuations of the coefficients were small in winter and large in spring and summer. The sensitivity coefficients in May showed that when SCF decreased by 1%, monthly runoff increased by 0.64%, with an inverse relationship between SCF and monthly runoff (Fig. 15a).

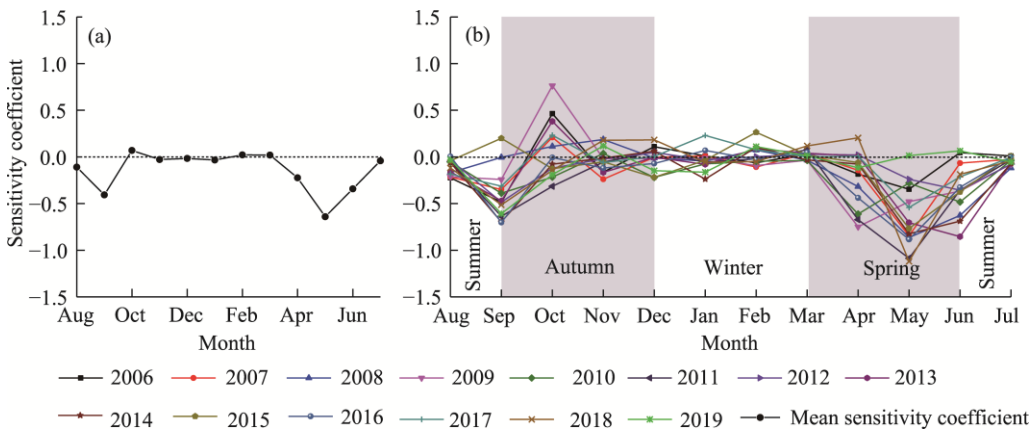

Fig. 15 Changes in the sensitivity coefficients of SCF to monthly runoff from 2006 to 2019. (a), multi-year monthly mean runoff; (b), monthly mean runoff at the annual scale.

Moreover, as shown in Figure 15b, the sensitivity coefficients of SCF to monthly runoff varied seasonally. Snow melted as the temperature increases in spring and summer, and SCF decreased while monthly runoff increased. In contrast, the fluctuation in the sensitivity coefficients of SCF to monthly runoff was small in winter and early autumn. Monthly runoff was greatly affected by SCF. A reduction in SCF had a significant effect on monthly runoff. This result is consistent with the study of Yang et al. (2003), who analyzed the relationship between SCA and runoff in Siberian watersheds from 1966 to 1999 and found a very strong relationship between SCA and runoff. They also quantified the seasonal cyclicity of SCA and runoff and determined a clear correspondence between the seasonal variation of SCA and runoff. In this study, we found that

low monthly runoff was associated with high SCA in winter and increased monthly runoff was related with decreased SCA in summer.

4.3 Uncertainty analysis

This study focused on the variations of SCF and the hydrological response of runoff to SCF change in the JRB under the background of climate change. Temperature, precipitation, elevation, slope and aspect were considered the factors affecting the change in snow cover. However, snowmelt is also related to wind speed, surface radiation, human activities and other factors (Nayak et al., 2010, 2012; Yang et al., 2020). In addition, there is a strong relationship between snow cover and runoff (Pederson et al., 2011; Barnhart et al., 2016; Li et al., 2017), and the extent to which snowmelt triggers runoff remains to be quantified. In view of the above problems, we will continue to investigate this topic in future studies.

5 Conclusions

The JRB on the northern slope of the Tianshan Mountains includes a typical river fed by glacial melting, which constitutes an important supply of water resources in nearby arid and semi-arid areas. Investigating the variations in snow cover and the response of runoff to these changes is of great significance for understanding the water cycle in alpine mountainous areas. Thus, based on meteorological and hydrological data and remote sensing snow cover data across the study area, the relationships among temperature, precipitation, snow cover and runoff were studied using various methods.

The variations of SCF showed obvious signs of periodicity, and the interannual variations have decreased slightly over time. There were obvious regional differences in the distribution of SCDs, with high SCDs being concentrated mainly in the southwestern and southern areas. Among the many factors driving such snow cover change, temperature exerted the greatest impact. Furthermore, after zoning the snow cover data by elevation, we found that SCF may be affected by snow (glaciers) above the elevation of 4200 m, and the annual variation trend was gentle; however, SCF fluctuated greatly at elevations below 4200 m. In addition, SCF varied with both slope and aspect. Specifically, slopes of 0°–10° were more conducive to snow cover, while slopes of 30°–40° were not conducive, and SCF was lower on the west- and north-facing aspects and higher on the south-facing aspects. The change in runoff was closely related to snow cover. A flood peak appeared when SCF decreased to its lowest value, and the runoff peak usually occurred at the end of August. After conducting a sensitivity analysis on SCF and monthly runoff, we discovered that SCF was negatively related to monthly runoff. Consequently, a reduction in SCF had a significant effect on the change in runoff. The results of this study can provide a reference for the simulation and prediction of snowmelt runoff in the future. However, there are still some other factors affecting the variation of snow cover that have not been quantified, so further research is needed in the next work.

Acknowledgements

This work was supported by the National Natural Science Foundation of China (41961002, U1603342) and the Natural Science Foundation Program of Xinjiang Uygur Autonomous Region (Special Training for Minorities) (2019D03004). The authors also thank the National Meteorological Information Center (NMIC) of the China Meteorological Administration (CMA), the Geospatial Data Cloud, the Bajiahu hydrological station in Xinjiang, the National Cryosphere Desert Data Center (NCDC), the National Snow and Ice Data Center (NSIDC) and the National Aeronautics and Space Administration (NASA) for providing datasets.

References

Barnhart T B, Molotch N P, Livneh B, et al. 2016. Snowmelt rate dictates streamflow. Geophysical Research Letters, 43(15): 8006–8016.

Chen X C, Zhang L P, Shan L J, et al. 2017. Flood prediction models and their application for the medium and small rivers in alpine area in Xinjiang. Arid Zone Research, 34(6): 1426–1435. (in Chinese)

Hall D K, Riggs G A. 2010. Accuracy assessment of the MODIS snow products. Hydrological Processes, 21(12): 1534–1547.

Hammond J C, Harpold A A, Weiss S, et al. 2019. Partitioning snowmelt and rainfall in the critical zone: effects of climate type and soil properties. Hydrology and Earth System Sciences, 23(9): 3553–3570.

Hao X H. 2021. A new MODIS snow cover extent product over China (2000–2020). National Tibetan Plateau Data Center (NTPDC) [data set]. [2021-07-17]. https://data.tpdc.ac.cn/en/.

Immerzeel W W, Droogers P, Jong S, et al. 2009. Large-scale monitoring of snow cover and runoff simulation in Himalayan river basins using remote sensing. Remote Sensing of Environment, 113(1): 40–49.

Jin H Y, Ju Q, Yu Z B, et al. 2019. Simulation of snowmelt runoff and sensitivity analysis in the Nyang River Basin, southeastern Qinghai-Tibetan Plateau, China. Natural Hazards, 99(2): 931–950.

Kendall M G. 1990. Rank correlation methods. British Journal of Psychology, 25(1): 86–91.

Khadka D, Babel M S, Shrestha S, et al. 2014. Climate change impact on glacier and snow melt and runoff in Tamakoshi basin in the Hindu Kush Himalayan (HKH) region. Journal of Hydrology, 511: 49–60.

Kour R, Patel N, Krishna A P. 2016. Assessment of temporal dynamics of snow cover and its validation with hydro-meteorological data in parts of Chenab Basin, western Himalayas. Science China Earth Sciences, 59(5): 1081–1094.

Kraaijenbrink P D A, Stigter E E, Yao T D, et al. 2021. Climate change decisive for Asia's snow meltwater supply. Nature Climate Change, 11(7): 591–597.

Li B F, Chen Y N, Chen Z S, et al. 2013. Variations of temperature and precipitation of snowmelt period and its effect on runoff in the mountainous areas of Northwest China. Journal of Geographical Sciences, 23(1): 17–30.

Li D Y, Wrzesien M L, Durand M, et al. 2017. How much runoff originates as snow in the western United States, and how will that change in the future? Geophysical Research Letters, 44(12): 6163–6172.

Li Q, Yang T, Zhou H F, et al. 2019. Patterns in snow depth maximum and snow cover days during 1961–2015 period in the Tianshan Mountains, Central Asia. Atmospheric Research, 228: 14–22.

Li Y P, Chen Y N, Li Z. 2020. Climate and topographic controls on snow phenology dynamics in the Tienshan Mountains, Central Asia. Atmospheric Research, 236: 104813, doi: 10.1016/j.atmosres.2019.104813.

Liu D, Zhong S B, Huang Q Y. 2015. Study on risk assessment framework for snowmelt flood and hydro-network extraction from watersheds. In: Bian F, Xie Y. Geo-Informatics in Resource Management and Sustainable Ecosystem. GRMSE 2015. Communications in Computer and Information Science, vol 569. Berlin and Heidelberg: Springer. https://doi.org/10.1007/978-3-662-49155-3_67.

Mann H B. 1945. Nonparametric tests against trend. Econometrica, 13(3): 245–259.

Miller S A, Mercer J J, Lyon S W, et al. 2021. Stable isotopes of water and specific conductance reveal complimentary information on streamflow generation in snowmelt-dominated, seasonally arid watersheds. Journal of Hydrology, 596: 126075, doi: 10.1016/j.jhydrol.2021.126075.

Moursi H, Kim D, Kaluarachchi J J. 2017. A probabilistic assessment of agricultural water scarcity in a semi-arid and snowmelt-dominated river basin under climate change. Agricultural Water Management, 193: 142–152.

Nagler T, Rott H, Malcher P, et al. 2008. Assimilation of meteorological and remote sensing data for snowmelt runoff forecasting. Remote Sensing of Environment, 112(4): 1408–1420.

Nayak A, Marks D, Chandler D G, et al. 2010. Long-term snow, climate, and streamflow trends at the Reynolds Creek Experimental Watershed, Owyhee Mountains, Idaho, United States. Water Resources Research, 46(6): W06519, doi: 10.1029/2008wr007525.

Nayak A, Marks D, Chandler D G, et al. 2012. Modeling interannual variability in snow-cover development and melt for a semiarid mountain catchment. Journal of Hydrologic Engineering, 17(1): 74–84.

Parajka J, Bezak N, Burkhart J, et al. 2019. MODIS snowline elevation changes during snowmelt runoff events in Europe. Journal of Hydrology and Hydromechanics, 67(1): 101–109.

Paudel K P, Andersen P. 2011. Monitoring snow cover variability in an agropastoral area in the Trans Himalayan region of Nepal using MODIS data with improved cloud removal methodology. Remote Sensing of Environment, 115(5): 1234–1246.

Pederson G T, Gray S T, Ault T, et al. 2011. Climatic controls on the snowmelt hydrology of the northern Rocky Mountains. Journal of Climate, 24(6): 1666–1687.

Qin J C, Su B D, Tao H, et al. 2021. Spatio-temporal variations of dryness/wetness over Northwest China under different SSPs-RCPs. Atmospheric Research, 259: 105672, doi: 10.1016/j.atmosres.2021.105672.

Saeed F H, Al-Khafaji M S, Al-Faraj F. 2022. Hydrologic response of arid and semi-arid river basins in Iraq under a changing climate. Journal of Water and Climate Change, 13(3): 1225–1240.

Steele C, Dialesandro J, James D, et al. 2017. Evaluating MODIS snow products for modelling snowmelt runoff: Case study of the Rio Grande headwaters. International Journal of Applied Earth Observation and Geoinformation, 63: 234–243.

Tahir A A, Chevallier P, Arnaud Y, et al. 2011a. Modeling snowmelt-runoff under climate scenarios in the Hunza River basin, Karakoram Range, Northern Pakistan. Journal of Hydrology, 409(1–2): 104–117.

Tahir A A, Chevallier P, Arnaud Y, et al. 2011b. Snow cover dynamics and hydrological regime of the Hunza River basin, Karakoram Range, Northern Pakistan. Hydrology and Earth System Sciences, 15(7): 2275–2290.

Tahir A A, Hakeem S A, Hu T, et al. 2017. Simulation of snowmelt-runoff under climate change scenarios in a data-scarce mountain environment. International Journal of Digital Earth, 12(8): 910–930.

Tan X J, Wu Z N, Mu X M, et al. 2019. Spatiotemporal changes in snow cover over China during 1960–2013. Atmospheric Research, 218: 183–194.

Tang G P, Li S P, Yang M Z, et al. 2019. Streamflow response to snow regime shift associated with climate variability in four mountain watersheds in the US Great Basin. Journal of Hydrology, 573: 255–266.

Uwamahoro S, Liu T, Nzabarinda V, et al. 2021. Modifications to snow-melting and flooding processes in the hydrological model-a case study in Issyk-Kul, Kyrgyzstan. Atmosphere, 12(12): 1580, doi: 10.3390/atmos12121580.

Wang X W, Xie H J, Liang T G. 2008. Evaluation of MODIS snow cover and cloud mask and its application in Northern Xinjiang, China. Remote Sensing of Environment, 112(4): 1497–1513.

Wu X J, Zhang W, Li H Y, et al. 2021. Analysis of seasonal snowmelt contribution using a distributed energy balance model for a river basin in the Altai Mountains of northwestern China. Hydrological Processes, 35(3): e14046, doi: 10.1002/hyp.14046.

Xiao X X, Zhang T J, Zhong X Y, et al. 2020. Spatiotemporal variation of snow depth in the Northern Hemisphere from 1992 to 2016. Remote Sensing, 12(17): 2728, doi: 10.3390/rs12172728.

Yang D Q, Robinson D, Zhao Y Y, et al. 2003. Streamflow response to seasonal snow cover extent changes in large Siberian watersheds. Journal of Geophysical Research-Atmospheres, 108(D18): 1–14.

Yang T, Li Q, Ahmad S, et al. 2019. Changes in snow phenology from 1979 to 2016 over the Tianshan Mountains, Central Asia. Remote Sensing, 11(5): 499, doi: 10.3390/rs11050499.

Yang T, Li Q, Chen X, et al. 2020. Improving snow simulation with more realistic vegetation parameters in a regional climate model in the Tianshan Mountains, Central Asia. Journal of Hydrology, 590: 125525, doi: 10.1016/j.jhydrol.2020.125525.

Yue S, Pilon P, Cavadias G. 2002. Power of the Mann-Kendall and Spearman's rho tests for detecting monotonic trends in hydrological series. Journal of Hydrology, 259(1–4): 254–271.

Zengir V S, Mahmoudi L, Rajabi K, et al. 2020. Monitoring and analysis of changes in the depth and surface area snow of the Mountains in Iran using remote sensing data. Journal of the Indian Society of Remote Sensing, 48(9): 1479–1494.

Zhang G Q, Xie H J, Yao T D, et al. 2014. Quantitative water resources assessment of Qinghai Lake basin using Snowmelt Runoff Model (SRM). Journal of Hydrology, 519: 976–987.

Zhang Q F, Chen Y N, Li Z, et al. 2020. Recent changes in water discharge in snow and glacier melt-dominated rivers in the Tienshan Mountains, Central Asia. Remote Sensing, 12(17): 2704, doi: 10.3390/rs12172704.